Optical Materials 69 (2017) 344–351

Contents lists available at ScienceDirect

Optical Materials

journal homepage: www.elsevier.com/locate/optmat

Effect of an electron beam irradiation on optical and luminescence properties of $LiBaAlF_6$ single crystals

I.N. Ogorodnikov [a, *], V.A. Pustovarov [a], S.I. Omelkov [b], M. Kirm [b]

[a] Ural Federal University, 19, Mira Street, 620002 Yekaterinburg, Russia
[b] Institute of Physics, University of Tartu, 1, W. Ostwaldi Street, 50411 Tartu, Estonia

ARTICLE INFO

Article history:
Received 5 March 2017
Received in revised form
18 April 2017
Accepted 26 April 2017
Available online 6 May 2017

Keywords:
Fluoride crystal LBAF
Optical absorption spectra
Luminescence spectra
Electron beam irradiation
Radiation defects

ABSTRACT

Paper reports the effect of a 10 keV, 110 keV and 10 MeV electron beam irradiation on optical and luminescence properties of $LiBaAlF_6$ (LBAF) single crystals at 10, 90, and 293 K. Five absorption bands at 2.0, 3.2, 4.3, 4.9 and 5.5 eV were revealed in irradiated crystals in the energy range of 1.2–9.5 eV. Several PL emission bands (1.7–1.8, 2.2 and 2.5–3.5 eV) related to defects were found in the luminescence spectra at room temperature, while only one luminescence band at $E = 2.2$ eV appears at $T = 90$ K in LBAF crystals after a 10 MeV electron bombardment. The PL excitation spectra and time-response for these emission bands were studied at 10, 90, and 293 K. Thermoluminescence (TL) of irradiated crystals was studied in the temperature range of 90–740 K. New TL glow peaks at 166, 530 and 670 K were revealed and their parameters were determined. Temperature dependence of relative photoluminescence yield recorded monitoring emission at the 1.87 and 2.23 eV in the temperature range from 130 to 450 K, were fitted using five quenching processes related to TL glow peaks revealed in our research. Significant similarity in the manifestation of radiation-induced defects for LBAF and previously studied $LiBaF_3$ single crystals is noted. The effect of an electron beam irradiation on optical and luminescence properties of LBAF single crystals and possible origin of the radiation defects were discussed.

1. Introduction

Optical materials on the basis of complex fluorides and double fluorine salts have many useful applications [1]. Among them, Li–Ba compounds are of particular interest for radiation detection because the ^{6}Li-isotope has advantages in interaction with thermal neutrons. There are two more crucial reasons. First, the Ba^{2+} ion is responsible for core-valence transitions F^- $2p \rightarrow Ba^{2+}$ $5p$ (so called 'cross-luminescence'), which features subnanosecond decay times. Second, a fluorine compound as a whole exhibits self-trapped exciton luminescence, which is not manifested under thermal-neutron irradiation. As both emissions give a response under gamma-ray excitation, this offer a unique opportunity for thermal neutron – gamma discrimination [2]. Some important impurities were tested as luminescence centers for $LiBaF_3$, for example Eu^{2+} [3] and Pb^+ [4,5].

Among the complex fluorides triple fluorine salts with common formula Li *Me* AlF_6 (*Me* = Ca, Sr, Ba) are distinguished. These optical crystals are used in laser technology for the far-ultraviolet spectral range. $LiCaAlF_6$ (LCAF) and $LiSrAlF_6$ (LSAF) crystals have been studied in sufficient detail, but $LiBaAlF_6$ (LBAF) crystals have attracted less attention. Luminescence and optical properties of undoped LBAF single crystals are reported in Refs. [6,7]. The band gap E_g was estimated as 12.1 eV in Ref. [6] and updated to more precise value of 12.3 eV in Ref. [8]. Both the cross-luminescence and intra-band luminescence of LBAF were reported in Refs. [6,7]. Because of partial overlapping between first core level and valence band of LBAF, their intensities and decay profiles are comparable. In a certain sense, the cross-luminescence in LBAF could be considered as a hole intra-band luminescence, as it is caused by radiative transitions of holes inside the 'complex' valence band. The luminescence spectroscopy of Pr^{3+}-doped LBAF crystals was previously reported in Ref. [9].

In this paper, we focus on the experimental study of the optical, luminescence and thermoluminescence properties of radiation defects in LBAF single crystals after electron beam irradiation at 10, 110 keV and 10 MeV. Despite the fact that the experimental technique used does not allow us to identify the origin of the created radiation defects, the spectroscopic 'portraits' of the defects

* Corresponding author.
E-mail address: i.n.ogorodnikov@gmail.com (I.N. Ogorodnikov).

http://dx.doi.org/10.1016/j.optmat.2017.04.060
0925-3467/

identified in this paper provide us with relevant information for future practical applications of this compound. We would like to emphasize also that our experimental research work does not intend to perform any quantum-chemical simulation of electronic structure of these defects.

2. Experimental details

All the examined LBAF crystals of high optical quality were grown from the melt of the corresponding fluorides (99.99%) utilizing the Bridgman technique at Institute of Geology and Mineralogy, Siberian Branch of Russian Academy of Sciences (Novosibirsk, Russia). The crystal growth technique was described in sufficient detail in Refs. [8,10]. The LBAF samples studied were in the form of optically transparent plane-parallel plates with the large surface polished to laser-grade quality, Fig. 1. Thickness of each sample is 1.8 mm. The orientation of the crystallographic axes of LBAF samples was arbitrary with respect to the polarization vector of the synchrotron radiation.

Photoluminescence (PL) excitation spectra in the ultraviolet (UV) and vacuum ultraviolet (VUV) energy regions (3.7–20 eV) were recorded at the SUPERLUMI experimental station of HASYLAB [11] upon selective photoexcitation with synchrotron radiation. The primary 2 m-vacuum monochromator equipped with two in situ interchangeable gratings, Al and Pt coated, had a typical resolution of 0.32 nm. The PL excitation (PLE) spectra were corrected to an equal number of incident photons using sodium salicylate — a luminophore with the energy-independent quantum yield over the studied spectral range. The 0.3 m ARC Spectra Pro-300i monochromator equipped with an R6358P (Hamamatsu) photomultiplier were used as a registration system. The measurements were performed at temperature of 10 K using a continuous-flow liquid helium cryostat mounted in the ultra-high vacuum chamber with a pressure of residual gases lower than 1×10^{-8} Pa.

Optical absorption spectra at 293 K were recorded at the laboratory of Solid State Physics of Ural Federal University by the means of a Heλios Alpha 9423UVA1002E spectrophotometer ($\lambda = 190–1000$ nm) equipped with the Vision 32 software. The deep-UV range (250–150 nm) was covered by the special setup in the Institute of Physics, University of Tartu, where a hollow cathode H_2 lamp and a VMR-2 spectrophotometer are used. The optical absorption coefficient k was calculated using the formula $k = -\ln(T)/l$, where T is the experimental optical transmittance and l is the thickness of the sample.

The PL characteristics under excitation in the UV energy region from 3.0 to 6.0 eV were recorded in the temperature range from 90 to 293 K at the laboratory of Solid State Physics of Ural Federal University. The 400 W deuterium discharge lamp with a continuous UV emission spectrum and the primary DMR-4 monochromator were used as an excitation source. The secondary DMR-4 monochromator and the R-6358-10 (Hamamatsu) photomultiplier tube were used as registration system. The PL excitation spectra were normalized to an equal number of photons incident on the sample using yellow lumogen with the energy-independent quantum yield over the studied spectral range.

Thermoluminescence (TL) glow curves were recorded using two different experimental setups.

The low-temperature (80–500 K) TL glow curves were recorded using a digital temperature controller providing a constant heating rate of 0.3 K/s. The samples were pre-irradiated by the radiation source based on BSW-2-type X-ray tube (Cu-anode, $U_a = 40$ kV, $I_a = 15$ mA). The TL glow curves were recorded in the spectral-integrated regime (2–6.2 eV) by FEU-39 photomultiplier tube. The sample was mounted in a vacuum cryostat with quartz windows and quick thermal response.

The high-temperature (293–750 K) TL glow curves were recorded in N_2 atmosphere at linear heating rate of 2 K/s using a System 310 TLD Reader after 10 keV electron beam exposure at 10 and 293 K. This procedure has also annealed the sample.

The irradiation with keV-range electrons was performed in the Institute of Physics, University of Tartu. The 10 keV electron beam excitation source has a continuous beam current which can be varied in the range from 50 nA to 1 μA. A typical beam spot area was about 0.5 mm^2. The 110 keV excitation source is the pulsed electron gun based on RADAN-303A type high voltage generator (designed at the Institute of Electrophysics of the Ural Branch of Russian Academy of Sciences, Yekaterinburg). The peak current density on the sample holder in our experiment was approximately ~60 A/cm^2 and the pulse FWHM was 800 ps. The high voltage generator provides pulse rate up to 5 pps. We used the beam with maximum electron energy of 110 keV to measure the pulse cathodoluminescence (PCL) data published in Ref. [7], which consequently irradiated the sample.

To study radiation defects created by relatively high-energy electrons we used microtron accelerator (M-20 type) at Ural Federal University. A 10 MeV electron beam was applied to the sample at room temperature, providing fluence of 5×10^{15} cm^{-2}.

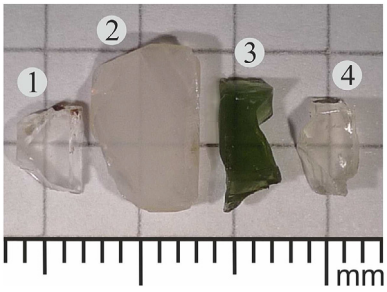

Fig. 1. Samples of LBAF crystals used in research work: pristine (1), irradiated by 110 keV electrons and then annealed in Ar at 600 °C for 2 h (2), irradiated by 10 MeV electrons (3), irradiated by 10 MeV electrons, then slowly heated to 700 K and immediately slowly cooled (10 K/min) (4). Thickness of each sample is 1.8 mm.

3. Experimental results

3.1. Optical absorption spectroscopy of defects

Fig. 2 shows the optical absorption spectra in the visible–UV energy range recorded for LBAF crystal at room temperature. Prior to electron bombardment, pristine crystal (Fig. 2, *a*, see also sample 1) was optically transparent in the investigated energy region of 1.5–6.0 eV, featuring no selective absorption bands. The effect of 10 keV electron irradiation on the optical absorption spectra of LBAF was already reported in Ref. [6] and proved to be insignificant. On the contrary, 110 keV beam (Fig. 2, *a*, curve *1*) led to a threefold increase in the absorption coefficient and induced light green coloration. We can clearly allocate at least five absorption bands at 2.0 (*A*), 3.2 (*B*), 4.3 (*C*), 4.9 (*D*) and 5.5 eV (*E*), which seemingly do not exhaust all the absorption bands in LBAF crystal. A subsequent annealing at 600 °C in argon atmosphere for two hours removed all coloration and selective absorption bands but rendered the crystal milky and poorly transparent (see sample 2). A 10 MeV electron bombardment led to even more significant increase in the absorption coefficient (Fig. 2, *b*, see also sample 3). In the energy region of 1.5–4.0 eV, we can observe the same absorption bands *A* and *B*, while above 4 eV the induced optical density is above the detection limit of our spectrometer (curve *3*). After slow heating to 700 K and immediate slow cooling in an argon atmosphere,

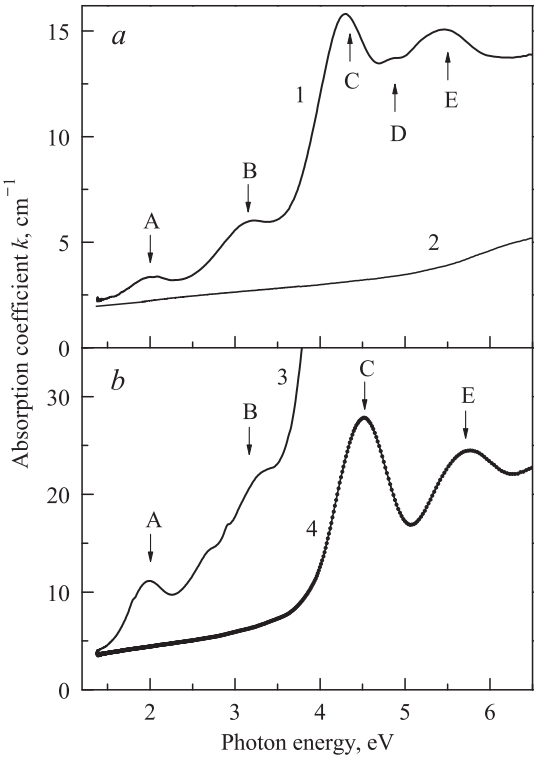

Fig. 2. Optical absorption spectra in the visible–UV energy range recorded at room temperature for LBAF crystals: (*a*) irradiated with an electron beam (E = 110 keV) (1) and pristine crystal (2); (*b*) irradiated with an electron beam (E = 10 MeV, fluence 5×10^{15} cm^{-2}) (3) and that annealed at 700 K after irradiation (2). The symbols A–E label the discussed absorption bands.

irradiated crystal has partially restored optical transparency (Fig. 2, *b*, curve *4*, see also sample 4). The *A* and *B* peaks are almost undetectable in the spectrum, while the *C* and *E* peaks have become clearly distinguishable and fully resolved. It is therefore possible that *C* and *E* bands are due to some persistent radiation defects which could not be reversed without severe thermal damage to the sample.

Fig. 3 demonstrates the optical absorption spectra in far ultraviolet energy range recorded at room temperature for LBAF crystal after a 110 keV electron bombardment (curve *1*) and that for pristine non-irradiated crystal (curve *2*). The absorption spectrum of irradiated crystal shows peak *E* at 5.5 eV, and in the energy region of 6–7 eV absorption coefficient remains approximately constant (13–14 cm^{-1}). Then, the absorption coefficient rises smoothly and reaches 30 cm^{-1} at about 8 eV. Above 8 eV, the absorption coefficient is too high to be determined by our instrumentation. As the absorption spectrum above 6 eV is not noticeably influenced by irradiation, the strong near-edge absorption probably arises due to defects created during crystal growth.

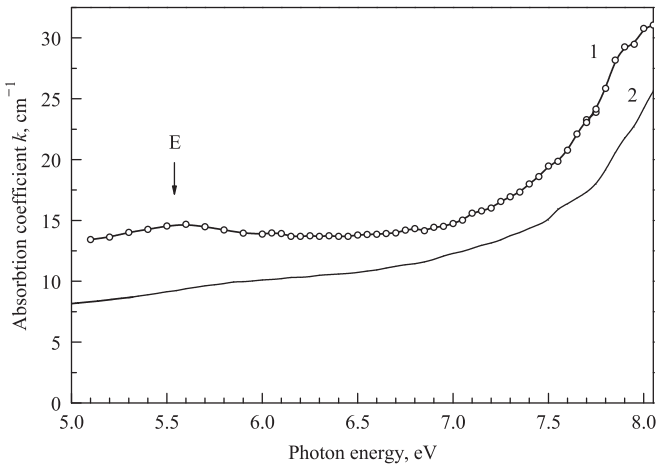

Fig. 3. Optical absorption spectra in far-ultraviolet energy region recorded at room temperature for LBAF crystal irradiated with an electron beam (E = 110 keV) (1) and that for the crystal annealed in an N_2 atmosphere at 700 K after irradiation with 10 keV electrons (2).

3.2. Luminescence spectroscopy of defects

Fig. 4 shows the normalized PL emission spectra of LBAF single crystal after irradiation with a 10 MeV electron beam, recorded at T = 10 K by the means of CCD camera upon selective excitation with synchrotron radiation at E_{ex}. The PL emission spectrum includes two partially overlapping broad bands at E_m = 2.15 and 2.42 eV. Both emission bands have FWHM = 0.3 eV. The relative intensities of these bands depend on the energy of exciting photons. At E_{ex} = 4.15 eV the spectrum is dominated by the 2.15 eV emission band, and at E_{ex} = 4.35 eV by the 2.42 eV emission band. At E_{ex} = 3.75 eV, both PL emission bands are low in intensity, but two new even lower intensity bands at 1.7–1.8 and 2.5–3.5 eV are detected in this spectrum.

Fig. 5 demonstrates PLE-spectra of LBAF single crystal after irradiation with a 10 MeV electron beam. They were recorded at T = 10 K monitoring emission at E_m = 2.15 and 2.45 eV. Both spectra are dominated by rather narrow PLE-peaks located at 4.1 and 4.3 eV, respectively. At higher energies there is a sharp decline in PLE intensity that reaches a minimum at 4.93 and 5.22 eV, respectively. In the energy region of 6–12 eV PLE-spectra are showing low intensity and little structure. The dominating PLE peaks are positioned well below E_g, coinciding with the strongest absorption peak *C*, so they can be assigned to a direct excitation of radiation-induced defect states. The absence of this luminescence in non-irradiated crystals [6] supports this assignment further.

Fig. 6 shows PL emission spectra recorded at 293 and 90 K for LBAF single crystal irradiated by 10 MeV electrons. Only one luminescence band peaking at E_m = 2.2 eV (FWHM = 2.1 eV) appears at T = 90 K for different excitation energies E_{ex}. This is the most intense band, excited at energies around E_{ex} = 4 eV. Other luminescence band peaking at 1.87 eV (FWHM = 2.0 eV) is

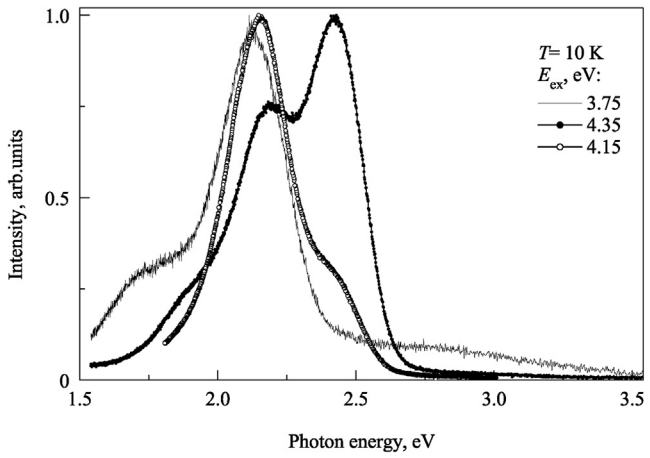

Fig. 4. The normalized PL emission spectra of LBAF single crystal after irradiation with a 10 MeV electron beam recorded at T = 10 K by the means of CCD camera upon selective excitation with synchrotron radiation at E_{ex}.

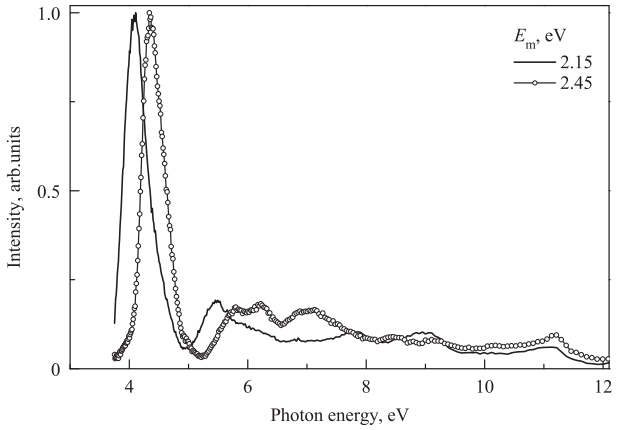

Fig. 5. PL excitation spectra of LBAF single crystal after irradiation with a 10 MeV electron beam, recorded at $T = 10$ K monitoring emission at $E_m = 2.15$ and 2.45 eV.

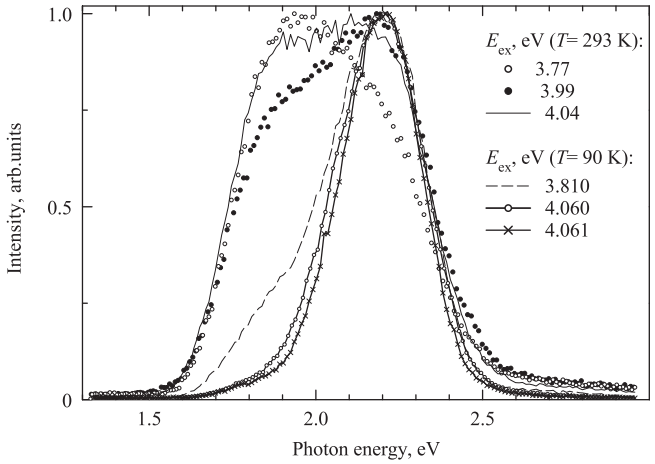

Fig. 6. PL emission spectra of LBAF single crystal after irradiation with a 10 MeV electron beam recorded at $T = 90$ and 293 K upon excitation at E_{ex}.

manifested more clearly at 293 K for $E_{ex} = 3.99–3.77$ eV.

Fig. 7 demonstrates PLE spectra of LBAF single crystal irradiated by 10 MeV electrons at room temperature recorded at 293 and 90 K

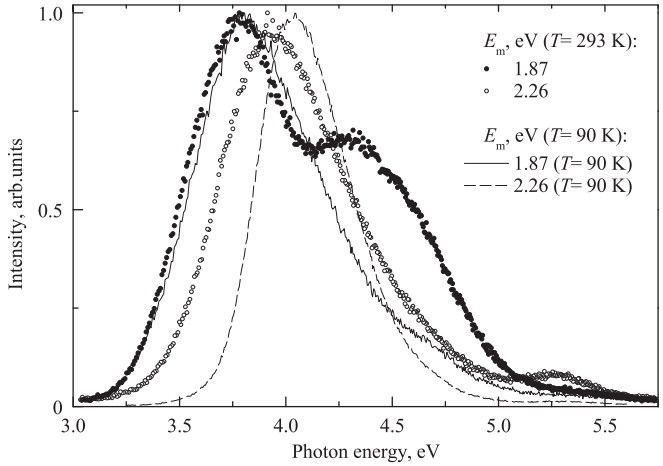

Fig. 7. PL excitation spectra of LBAF single crystal after irradiation with a 10 MeV electron beam recorded at $T = 90$ and 293 K monitoring emission at E_m.

monitoring emission at $E_m = 1.87$ and 2.26 eV. One can identify two groups of PLE-bands: one of them is located in the energy range from $E_{ex} = 3.25–3.8$ eV, while the other is located above $E_{ex} = 3.8$ eV. There is also a low-intensity PLE-band at $E_{ex} = 5.25$eV. At $T = 293$ K, PLE spectrum recorded monitoring emission at $E_m = 1.87$ eV, comprises two PLE-bands at $E_{ex} = 3.8$ and 4.34 eV. At $T = 90$ K, the 3.8 eV band dominates PLE spectrum. The PLE spectrum recorded monitoring emission at 2.2 eV, comprises two bands with maxima at $E_{ex} = 3.9$ and 5.3 eV at $T = 293$ K. At $T = 90$ K, PLE maximum is shifted to $E_{ex} = 4.04$ eV.

3.3. Thermoluminescence of defects

Fig. 8 shows a high-temperature spectral-integrated thermoluminescence glow curve recorded for LBAF crystal at linear heating (2 K/s) after an X-rays exposure and subsequent 10 keV electron bombardment at 293 K. The TL glow curve comprises two partially overlapping broad complex peaks at 530 and 670 K. High-temperature peak at 670 K dominates the TL glow curve. Another TL peak at 530 K reaches only about 30% of intensity in comparison with that for the dominant TL peak at 670 K. From Fig. 2 it follows that annealing at 700 K leads to thermal bleaching the A and B optical absorption bands. This means that the TL peaks at 530 and 670 K may be caused by annealing of color centers being responsible for optical absorption bands A and B.

To approximate the experimental data we used the sum of the four TL peaks of the first-order kinetics.

$$I(T) = \sum_{i=1}^{4} I_i S_i \exp\left(-\frac{E_i}{k_B T} - \frac{S_i}{\beta} \int_{T_0}^{T} \exp\left(-\frac{E_i}{k_B T} \right) dT \right), \quad (1)$$

where I_i is a relative contribution of i-process to TL glow curve; S is a preexponential factor; E is an activation energy; k_B is the Boltzmann constant; β is a heating rate; T_0 is an initial temperature. We would like to mention two important facts: first, deconvolution using formula (1) does not account for possible interaction between defects, so the calculation results are affected by the partial overlapping the TL glow peaks; second, we tested different values of the kinetics order, however only the first-order kinetics provided best approximation.

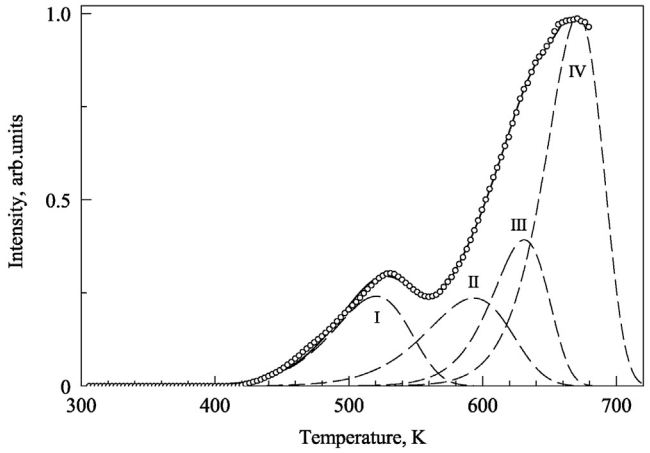

Fig. 8. The high-temperature spectral-integrated thermoluminescence glow curve recorded for LBAF crystal at linear heating (2 K/s) after a 10 keV electron bombardment and X-rays exposure at 293 K. Open circles represent the experimental data, smooth solid curve shows the best fit result, dashed curves with the Roman numerals I–IV represent constituent individual TL glow peaks.

Approximation quality was evaluated using standard criterion FOM (Figure Of Merit)

$$\text{FOM}\ [\%] = \frac{\sum_i |y_i - y(T_i)|}{\sum_i y_i} \times 100\%, \quad (2)$$

here, y_i is the experimental data in the channel i, $y(T_i)$ and T_i are the values of the approximation function and temperature in the center of the channel i. The best approximation of the experimental data on the high-temperature spectral-integrated TL was achieved with FOM = 2.37%.

Fig. 8 and Table 1 present the four deconvoluted TL glow peaks and their best fit parameters. Due to technical limitations, the high-temperature slope of TL glow peak IV (Fig. 8) could not be properly registered in our high-temperature measurements, so the parameters of the peak IV (Table 1) are rather speculative. However, lower values of thermal activation parameters for the peaks I and IV alongside with the first order kinetics may be considered as indirect evidence of radiation-defect annealing at these temperatures.

Fig. 9 (curve 3) shows spectral-integrated TL glow curve recorded in the temperature range of 90–293 K for LBAF crystal at linear heating (0.3 K/s) after a 10 MeV electron bombardment at 293 K and subsequent X-rays exposure at T_0 = 90 K. The best approximation of the experimental data was achieved with FOM = 3.99%. Two of the most intense TL peaks at 130 and 192 K with activation energies of 0.22 and 0.33 eV have been reported in our previous work [6]. Fig. 9 shows only the next intense TL glow peak at 166 K, which was found in this paper. The 166 K peak has second-order kinetics (E = 0.25 eV, S = 1.2 MHz) and partially overlaps the peak at 192 K. It should be noted that these parameters can not qualify for accuracy, since the TL glow peak at 166 K is overlapping with the dominant peaks at 130 and 192 K. However, experimental data certainly testify in favor of presence of new TL peak at 166 K.

3.4. Temperature dependence of emission intensity

Fig. 9 demonstrates temperature dependences of relative photoluminescence yield $\eta(T)$ for LBAF single crystal after irradiation with a 10 MeV electron beam at room temperature. These dependences were recorded monitoring emission at E_m = 1.87 (TQ1) and 2.23 eV (TQ2) upon excitation at E_{ex} = 3.77 and 4.04 eV. The $\eta(T)$ dependence in each emission band increases dramatically with decreasing temperature of the crystal. From Fig. 9 it is seen that the $\eta(T)$ dependence is different for different emission bands. Assuming the Mott-Seitz mechanism [12,13] of thermal quenching, superposition of five thermal quenching processes was used to approximate both temperature dependences.

Table 1
Best fit parameters (first order kinetics) for the high-temperature spectral-integrated thermoluminescence glow curve recorded for LBAF crystal at linear heating (2 K/s) after a 10 keV electron bombardment and X-rays exposure at 293 K.

Parameter	TL glow peak			
	I	II	III	IV
T_m, K	520.0	593.3	630.8	671.0
I_m, a.u.	23.7	23.2	38.9	98.4
S, GHz	0.002	720	3300	0.004
E_a, eV	0.78	1.62	1.81	0.92

Note: T_m is a temperature position of the TL glow peak; I_m is a peak intensity normalized to 100 conventional units at the maximum of the observed TL glow curve; S is a preexponential factor; E_a is an activation energy.

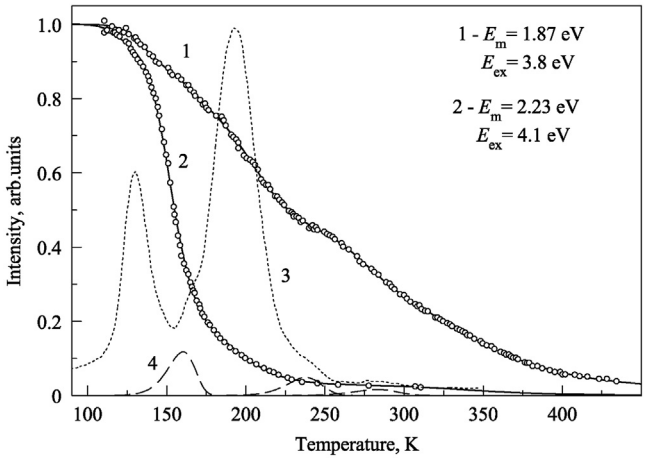

Fig. 9. Temperature dependence of PL emission yield for LBAF single crystal after irradiation with a 10 MeV electron beam recorded monitoring emission at E_m upon excitation at E_{ex} (1, 2). Open circles represent the experimental data, smooth lines show the best fit results. Spectral-integrated TL glow curve (3) was recorded at heating rate of 0.3 K/s. Curve 4 corresponds to new individual TL glow peaks at 160.4, 237.8, 283.0 K discovered as a result of fitting.

$$\eta(T) = I(T)/I_{max} = \sum_{i=1}^{5} \frac{I_{0i}}{1 + W_i \exp(-E_i/k_B T)}, \quad (3)$$

where E_i is an activation energy for thermal quenching, W_i is a dimensionless preexponential factor; i is an index to indicate a quenching process; I_{0i} is a relative contribution of i-process to the observed PL emission. For each i-process, we determined the quenching temperature $T_{1/2}$, at which the emission intensity of the process decreases to 50% of its initial intensity I_{0i}. From the Mott law we can derive a useful formula to estimate $T_{1/2}$.

$$T_{1/2} = E/k_B \ln W. \quad (4)$$

Table 2 presents the best fit parameters for a temperature dependence of the luminescence yield recorded monitoring

Table 2
Best fit parameters for a temperature dependence of the luminescence yield recorded monitoring emission at E_m = 1.87 and 2.23 eV, and a TL glow curve shown in Fig. 9.

Parameter	Quenching process, i				
	1	2	3	4	5
E_m = 1.87 eV (TQ1)					
$T_{1/2}$, K	136.5	170.1	209.2	277.6	346.3
$I_0 \times 100$ %	12.9	12.8	30.9	14.9	26.8
ln W	17.43	17.36	16.08	21.66	11.09
E, meV	205	254	290	520	430
E_m = 2.23 eV (TQ2)					
$T_{1/2}$, K	119.6	153.3	202.8	285.0	345.0
$I_0 \times 100$ %	6.5	81.1	12.6	>0.1	2.7
ln W	19.99	20.07	16.43	22.41	13.40
E, meV	206	265	287	550	400
Spectral-integrated TL					
T_m, K	130.0	160.4	192.6	283.0	–
b	1.6	1.0	1.7	1.2	–
E_a, meV	204	250	295	540	–

Note. Parameters were determined for each i-process: I_{0i} is a relative contribution of i-process to the observed PL emission; W is a dimensionless preexponential factor and E is an activation energy for thermal quenching process; the quenching temperature $T_{1/2}$, at which the emission intensity of the process decreases to 50% of its initial intensity I_{0i}. Parameters were determined for each TL glow peak: T_m is a temperature position; E_a is an activation energy; b is a kinetic order.

emission at 1.87 and 2.23 eV. Approximation quality (Table 2) for each curve was assessed using FOM-criterion in the same manner as it was done for thermoluminescence (Eq. (2)). The best approximations were achieved with FOM = 0.67% (TQ1), 1.24% (TQ2), and 2.32% (TL). The determinacy factors were $R^2 = 0.999$ (TQ1, TQ2) and 0.998 (TL).

Temperature dependence of relative photoluminescence yield recorded monitoring emission at 1.87 emission band (TQ1) was fitted by five quenching processes. The $T_{1/2}$ temperatures for these processes are located in the temperature range from 130 to 290 K, and their relative contributions are comparatively high: 12–15 (i = 1, 2, 4), 26.8 (i = 5), and 30.9% (i = 3). Owing to this, the temperature dependence of $\eta(T)$ is a smoothly decaying curve in the temperature range from 130 to 400 K, Fig. 9.

The $\eta(T)$ dependence for the 2.2 eV emission band (TQ2) was also fitted by five quenching processes, however the second process dominates, causing a 81.1% contribution to the observed PL intensity. The first and third processes determine 6.5 and 12.6%, respectively. The fourth and fifth most low-intensity processes are located at temperatures above 200 K and determine together less than 2.8%. The background level is 0.5%.

The first three processes that determine temperature quenching of both emission bands are apparently the same. This is supported by the similarity between the activation energies of the quenching processes for both PL emission bands, Table 2. From formula (4) it follows that all the differences in the temperature positions ($T_{1/2}$) of the processes are determined by differences in the W-factors. W-factor is the ratio of probabilities for non-radiative (A_{NR}) and radiative (A_R) processes [12,13].

$$W = A_{NR}/A_R. \quad (5)$$

From Table 2 it is evident that the 2.23 eV emission band is characterized by elevated values of W-factors. Two reasons can be assumed. It is either increased values for the probability of non-radiative processes A_{NR} or slower time-response of the 2.23 eV luminescence ($A_R = 1 / \tau$).

It is worth mentioning that the temperature range of $T_{1/2}$ match well the temperature positions of the TL glow peaks at 130 and 192 K reported in Ref. [6]. Three new low-intensity TL glow peaks at 160.4, 237.8, 283.0 K were discovered in our work, Fig. 9. Two of them, namely TL glow peaks at 160 and 283 K coincide well the quenching processes i = 2 ($T_{1/2}$ = 153–170 K) and i = 4 ($T_{1/2}$ = 277–285 K). The TL glow peak at 237.8 K (E_a = 0.48 eV) was also detected at deconvolution, but we did not find its connection with the thermal quenching processes. This may be considered as indirect evidence that some quenching processes do not realize the Mott-Seitz mechanism, but they might be due to depopulation of the ground level of the luminescence center (external quenching mechanism). In this case Eq. (3) can also be valid, but the E_i has another meaning — the activation energy for depopulation of the center.

3.5. Time response of the luminescence

Fig. 10 shows PL decay kinetics recorded for LBAF single crystal at 10 K monitoring emission at E_m = 1.82 and 2.16 eV upon excitation at E_{ex} = 3.76 and 4.13–4.76 eV. Fast decay component has lifetime of about 10 ns, which correlates with our previous data on pulse cathodoluminescence. From Ref. [7] it follows that the 2.15 and 2.42 eV PCL emission bands at T = 78 K are characterized by two decay components with the lifetimes of 14.5 and 2.7 ns. It is worth mentioning that the 2.42 eV emission band with the lifetime of 2.7 ns and the dominant excitation peak in the excitonic region, has been studied previously in Ref. [6]. In this paper we deal with

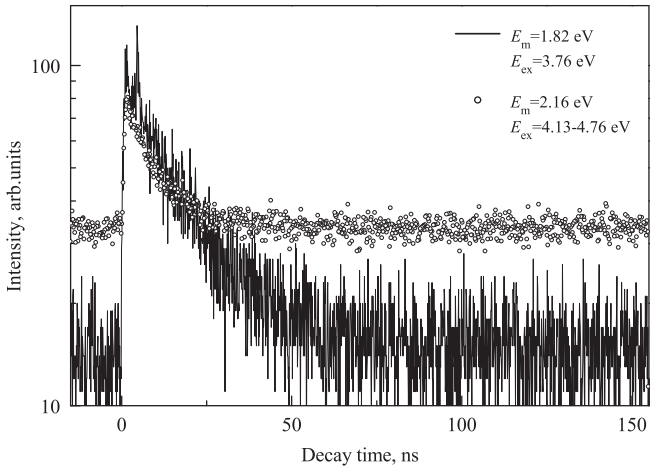

Fig. 10. PL decay kinetics recorded for LBAF single crystal at 10 K monitoring emission at E_m upon excitation at E_{ex}.

the 2.42 eV emission band with the lifetime of 2.7 ns that exhibits the principal excitation band at 3.8–3.9 eV, and no PLE band was found in the excitonic energy range, Fig. 7.

The double emission band at 1.8–2.5 eV is likely to be caused by the irradiation-induced defects. The explanation for that lies in poor radiation stability of studied compound under electron beam. It was already shown [6], that under continuous irradiation by 10 keV electron beam the emission intensity quickly drops with time, and at lower temperatures this effect is much stronger.

3.6. Discussion

Analysis of the above results show that the absorption and PL emission spectra reveal lattice defects, which were created in LBAF crystal during an electron beam irradiation. We are not aware of other experimental works on defects in LBAF single crystals, but such results are reported for the related $LiBaF_3$ crystal. In this connection, it makes sense to discuss our experimental results on LBAF in comparison with published data on $LiBaF_3$.

Our preliminary results [8] clearly indicate that a broad PL emission band peaking at 4.3 eV in LBAF crystals is due to radiative annihilation of self-trapped excitons (STE). At low temperatures (T = 10 K), this emission band dominates the PL spectrum, while at room temperature, this band has negligible intensity. From a general point of view, this results does not exclude the existence of self-trapped holes (STH) in irradiated LBAF-crystals.

Indeed, an X-ray irradiation of related $LiBaF_3$ crystal at T = 10 K leads to the creation of STH in the form of molecular F_2^- ion, i. e. V_k center. Such V_k center occupies the fluorine site and it is oriented along [1 1 0] crystallographic direction [14,15]. The radiation defects anneal in a multi-stage process accompanied with thermoluminescence at 20, 46, 105, 130, 170, 210 and 270 K. The TL glow peak at 20 K arises from the delocalization of H-centers. Two TL glow peaks at 105 and 130 K are due to 60° and 90° migration hops of V_k-centers [15,16].

Comparing these published data with our results for a 10 and 110 keV electron beam excitation, we can draw that all the spectroscopic steady-state manifestations of hypothetical STHs in LBAF crystals should be expected only at low temperatures. Therefore, the low-temperature TL glow peaks in the temperature range of 100–250 K (Fig. 9) can be tentatively attributed to annealing of intrinsic lattice defects (V_k or H-centers) in LBAF single crystals. In contrast, all the optical absorption bands and TL glow curves registered in LBAF above room temperature have different origin.

It is known [17] that radiation defects in alkali halide crystals can be created either through the decay of electronic excitations into defects (subthreshold mechanism) or through the impact mechanism. Most likely that the radiation defects in LBAF crystals upon an electron beam irradiation at $E = 110$ keV and 10 MeV are induced mainly through the impact creation mechanism. From a general point of view, the fluorine ion vacancies can be formed in the anion sublattice, followed by the formation of F-centers ($V_F^+ + e^-$), and the lithium ion vacancies can be formed in the cation sublattice with subsequent formation of V_{Li}-centers ($V_{Li}^- + h^+$).

Let us first mention the available data on the related $LiBaF_3$ crystal. The X-ray irradiation of $LiBaF_3$ leads also to the formation of the F-type color centers, which are the main radiation defect created by X-rays in $LiBaF_3$ at $T = 293$ K; this center manifests itself in electron paramagnetic resonance and has g-tensor with main axis along the [1 0 0] direction of the crystal [18,19]. The model of the center has been supported by magneto-optical studies of defects and recombination luminescence at 4.2 and 293 K [20]. Three optical absorption bands at 2.9 eV (430 nm), 3.8 eV (320 nm) and 4.6 eV (270 nm) induced by X-ray irradiation at 300 K are due to F-type centers [15,21–23]. The main absorption band of the F-type centers at 2.9 eV in $LiBaF_3$ crystals is subject to thermal quenching in the temperature range of 320–500 K [24].

Five absorption bands at 2.0 (*A*), 3.2 (*B*), 4.3 (*C*), 4.9 (*D*) and 5.5 eV (*E*) were revealed in LBAF single crystals irradiated by an 110 keV or 10 MeV electron beam, Fig. 2. The *A*-, *B*-, and *D*-absorption bands in LBAF crystals are subject to thermal annealing at temperatures below 700 K. It makes sense to treat them analogously to the three absorption bands of F-type color centers detected in $LiBaF_3$ crystals. On the other hand, the higher temperature *C*- and *E*-defects that dominate the absorption spectrum (Fig. 2) after irradiation with an 10 MeV electron beam, should be attributed to the much greater structural damage of LBAF lattice. It is still premature at this stage to discuss the origin of the *C*- and *E*-defects in LBAF any further.

Thermal annealing of the defects in LBAF crystals leads to the appearance of TL in the temperature range of 400–700 K (Fig. 8). Reduced values of thermal activation parameters for the TL glow peaks I and IV as compared to the other peaks (Table 1) may indirectly indicate the presence of the anion diffusion in LBAF crystals.

Indeed, such anion diffusion above room temperature takes place in $LiBaF_3$ crystals and leads to thermally stimulated destruction of the F-type and other centers [24]. The appropriate TL glow peaks in $LiBaF_3$ are low in intensity, and they also have reduced values of the process activation energies and preexponential factors that was interpreted in Ref. [23] as the presence of moving anion vacancies being responsible for a random walk of the F-type centers. In course of the random walk of the F-centers both the creation of aggregate F-centers and annihilation with some complementary radiation defects might take place [23]. Depending on the impurity composition two alternative mechanisms are involved in the annealing of color centers. It is proposed that either the anion vacancy governs migration of F-centers resulting in recombination with complementary defects, or the thermal delocalization of radiation creates fluorine (F_i) interstitials captured by anti-site defects followed by recombination with all kinds of complementary F-type centers are responsible for the recombination of radiation defects above room temperature [25]. From the trap spectroscopy it follows that the decay of the F-type centers is governed by interaction of mobile anion vacancies with F_A and F-centers, leading to both the hopping migration and recombination of F-centers and the thermally stimulated dissociation of the F_A centers [26].

The PL emission bands in LBAF crystals (Figs. 4 and 6) are substantially different from the intrinsic PL emission band at 4.3 eV. They are likely caused by different lattice defects in LBAF crystals. A large variety of PL emission bands in LBAF can be explained by two different reasons.

First, a tunneling recombination process between closely-spaced electron and hole trapping centers may be responsible for a slowly-decaying PL emission band. In fact, a long-time temperature-independent afterglow in $LiBaF_3$ at 4.1 eV is due to the tunneling recombination between closely-spaced electron and hole centers. The likely recombination partners are F-type electron centers and the V_k as well as probably O^{2-} hole centers [27].

Second, defect formation in a crystal depends strongly on the conditions of crystal growth and preparation of the samples. Electron-irradiation of LBAF can induce different F-types defects. The published data on $LiBaF_3$ discussed the F-type color centers in the form of F, F_2, F_2^+, F_3 and F_3^+ with different absorption bands [28]. A room temperature electron irradiation of crystals favors the formation of different kinds of F-aggregate centers. In particular, the formation of F_2^+ centers with an absorption band at 1.9 eV (632 nm) and a corresponding emission band at 1.7 eV (702 nm) was observed in $LiBaF_3$ crystals [29].

Therefore, there is a significant similarity in the manifestation of radiation-induced defects for $LiBaF_3$ and LBAF single crystals. Based on the analogy of the available data discussed above, we have made only preliminary discussion about the origin of the radiation defects induced by an electron beam in LBAB single crystals. However, a more detailed discussion of LBAF defects requires further investigation.

4. Conclusions

Research work is devoted to the study of the optical and luminescence properties of radiation defects created in LBAF crystals by irradiation with the 10 keV, 110 keV and 10 MeV electron beams. Most essential results obtained for irradiated crystals are as follows. Five absorption bands at 2.0, 3.2, 4.3, 4.9 and 5.5 eV were revealed in the optical absorption spectra in the visible-UV-VUV energy ranges (1.2–9.5 eV). Several PL emission bands (1.7–1.8, 2.2 and 2.5–3.5 eV) related to defects were found at room temperature in the luminescence spectra. In contrast, only one luminescence band at $E = 2.2$ eV appears at $T = 90$ K in LBAF crystals after a 10 MeV electron bombardment. The PL excitation spectra and time-response for these emission bands were studied as well. The nanosecond decay kinetics of low-temperature ($T = 10$ K) photoluminescence correlates with our previous data on pulsed cathodoluminescence. Thermoluminescence of irradiated crystals was studied in the temperature range of 90–740 K. New TL glow peaks at 166, 530 and 670 K were revealed and their parameters were determined. Temperature dependence of relative photoluminescence yield recorded monitoring emission at the 1.87 and 2.23 eV in the temperature range from 130 to 450 K, were fitted using five quenching processes related to TL glow peaks revealed in our research. We note a significant similarity in the manifestation of radiation-induced defects in LBAF and previously investigated $LiBaF_3$ single crystals, where the radiation defects are induced after irradiation with electron beam through the impact creation mechanism. On the basis of this similarity, we make preliminary conclusions about the origin of the defects induced by the electron beam in LBAF crystals. However, a more detailed discussion of LBAF defects requires further investigation.

Acknowledgments

This work was partially supported by the Ministry of Education and Science of the Russian Federation (Contract No.02.A03.21.0006) (the basic part of the government mandate), the Center of Excellence “Radiation and Nuclear Technologies”

(Competitiveness Enhancement Program of Ural Federal University, Russia), HASYLAB DESY (Project No.20110843), Estonian Research Council (projects IUT2-26 and PUT1081). We are grateful to Ludmila Isaenko for providing the crystals examined and Eugene Vasilchenko for recording a high-temperature TL glow curve.

References

[1] W. Pies, A. Weiss, in: Key Elements: F, Cl, Br, I, Vol. 7a of Landolt-börnstein - Group III Condensed Matter, Springer, Berlin Heidelberg, 1973, pp. pp.254–265.
[2] M.J. Knitel, P. Dorenbos, J.T.M. de Haas, C.W.E. van Eijk, in: Proceedings of the International Conference on Inorganic Scintillators and Their Applications, Delft University Press, Delft, The Netherlands, 1995, pp. 81–83.
[3] A. Meijerink, J. Lumin. 55 (3) (1993) 125.
[4] L. Prado, N.D. Vieira Jr., S.P. Morato, J.Y. Gesland, Solid State Commun. 87 (1) (1993) 41.
[5] L. Prado, N.D. Vieira Jr., S.L. Baldochi, S.P. Morato, J.P. Deniss, N. Tercier, B. Blanzat, J. Phys. Chem. Solids 57 (4) (1996) 413.
[6] S.I. Omelkov, M. Kirm, E. Feldbach, V.A. Pustovarov, S.O. Cholakh, L.I. Isaenko, J. Phys. Condens. Matter 22 (29) (2010) 295504 (8).
[7] I.N. Ogorodnikov, S.I. Omelkov, V.A. Pustovarov, A. Kasikov, M. Kirm, Opt. Mater. 39 (2015) 52.
[8] V.A. Pustovarov, I.N. Ogorodnikov, S.I. Omelkov, D.A. Spassky, L.I. Isaenko, J. Opt. Soc. Am. B-Opt. Phys. 31 (8) (2014) 1926.
[9] S.I. Omelkov, V. Kiisk, I. Sildos, M. Kirm, V. Nagirnyi, V.A. Pustovarov, L.I. Isaenko, S.I. Lobanov, Radiat. Meas. 56 (2013) 49.
[10] A.A. Merkulov, L.I. Isaenko, S.I. Lobanov, D.Y. Naumov, N.V. Kuratieva, Acta Crystallogr. C64 (7) (2008) i66.
[11] G. Zimmerer, Radiat. Meas. 42 (4–5) (2007) 859.
[12] N.F. Mott, R.W. Gurney, Electronic Processes in Ionic Crystals, Oxford University Press, London, 1948.
[13] D. Curie, Luminescence in Crystals, Wiley, NewYork, 1963.
[14] K. Somaiah, M.V. Narayana, L.H. Brixner, Mater. Chem. Phys. 24 (4) (1990) 353.
[15] I. Tale, H.-J. Fitting, P. Kulis, V. Ogorodnik, U. Rogulis, M. Springis, V. Tale, J. Trokšs, A. Veispāls, Radiat. Eff. Defect. Solid. 149 (1–4) (1999) 269.
[16] P. Kulis, I. Tale, I. Gromuls, M. Nikl, N. Ichinose, K. Shimamura, Radiat. Meas. 38 (4–6) (2004) 723.
[17] Ch B. Lushchik, A. Ch Lushchik, Decay of Electronic Excitations with Defect Formation in Solids, Nauka, Moscow, 1989.
[18] U. Rogulis, V. Ogorodnik, I. Tale, A. Veispals, Radiat. Eff. Defect. Solid. 157 (6–12) (2002) 699.
[19] A. Fedotovs, E. Elsts, U. Rogulis, A. Gulans, I. Tale, M. Nikl, N. Ichinose, K. Shimamura, Phys. Status Solidi C. 4 (3) (2007) 1284.
[20] U. Rogulis, J.-M. Spaeth, I. Tale, M. Nikl, N. Ichinose, K. Shimamura, Radiat. Meas. 38 (4–6) (2004) 663.
[21] I. Tale, P. Kulis, U. Rogulis, V. Tale, J. Trokss, A. Veispals, M. Barboza-Flores, H.J. Fitting, J. Lumin. 72–74 (1997) 722.
[22] P. Kulis, I. Tale, M. Springis, U. Rogulis, J. Trokss, A. Veispals, H.-J. Fitting, Radiat. Eff. Defect. Solid. 149 (1–4) (1999) 97.
[23] P. Kulis, I. Tale, M. Springis, U. Rogulis, A. Veispals, H.-J. Fitting, Radiat. Eff. Defect. Solid. 155 (1–4) (2001) 77.
[24] V. Ziraps, P. Kulis, I. Tale, A. Veispals, Radiat. Eff. Defect. Solid. 149 (1–4) (1999) 183.
[25] P. Kulis, M. Springis, I. Tale, Radiat. Eff. Defect. Solid. 157 (6–12) (2002) 737.
[26] P. Kulis, I. Tale, G. Rudlof, Radiat. Prot. Dosim. 100 (1–4) (2002) 167.
[27] I. Tale, M. Springis, U. Rogulis, V. Ogorodnik, P. Kulis, V. Tale, A. Veispals, H.J. Fitting, Radiat. Meas. 33 (5) (2001) 751.
[28] L. Prado, L. Gomes, S.L. Baldochi, S.P. Morato, N.D. Vieira Jr., J. Phys. Condens. Matter 10 (1998) 8247.
[29] L. Prado, L. Gomes, S.L. Baldochi, S.P. Morato, N.D. Vieira Jr., Radiat. Eff. Defect. Solid. 149 (1–4) (1999) 249.